Incoherent light transport in an anisotropic random medium: A probe of human erythrocyte aggregation and deformation

C. Baravian,[1,*] F. Caton,[2] J. Dillet,[1] G. Toussaint,[3] and P. Flaud[3]
[1]*Laboratoire d'Energétique et de Mécanique Théorique et Appliquée, CNRS UMR 7563, Nancy University, 2 Avenue de la Forêt de Haye, B.P. 160, 54504 Vandoeuvre Cedex, France*
[2]*Laboratoire de Rhéologie, BP 53 Domaine Universitaire 1301 rue de la Piscine 38041, Grenoble Cedex 9, France*
[3]*Laboratoire Matière et Systèmes Complexes CNRS UMR 7057, Bâtiment Condorcet 10 rue Alice Domont et Léonie Duquet, 75205 Paris cedex 13, France*
(Received 30 May 2006; revised manuscript received 2 April 2007; published 31 July 2007)

This paper investigates the flow induced disaggregation, deformation and orientation of several modified human red blood cells suspended in concentrated, physiological like conditions (volume fraction in erythrocytes of 0.4). The aim is to determine simultaneously, and under flow, the aggregate sizes as well as the deformation and orientation of the cells. The measurement method uses steady, incoherent, unpolarized light transport while the sample is sheared in a flow cell controlled by a rheometer. Several blood samples were prepared to alter the erythrocyte's aggregating, deformability and shape properties. The measurements using these samples show a clear relationship between the intrinsic properties of the cells and the evolution of aggregate sizes, average cell orientation and anisotropy as a function of the applied shear, which may lead to clinical applications. In other words, the careful analysis of the incoherent light transport in concentrated media provides quantitative insight into their microscopic details. In particular, the topological properties (average anisotropy and orientation) and size of the suspended objects can be determined.

DOI: 10.1103/PhysRevE.76.011409 PACS number(s): 83.80.Hj, 42.25.Dd, 83.85.Ei, 87.19.Uv

I. INTRODUCTION

Incoherent light transport in turbid media has developed steadily in the past 30 years or so [1–8], even though coherent techniques have known a greater success in the past decades [9–11]. Originally, the development of incoherent light transport techniques was motivated by the determination of the light transport properties of a turbid medium so that embedded objects could be detected through optical tomography (e.g. [12–15]). Today, there is a continuing emphasis on the development of noninvasive measurement tools that may probe a very large number of materials, such as biological tissues [16], colloidal suspensions [17], emulsions [18] or atmospheric particles [7] with a renewed interest for incoherent techniques [17–19]. Recently, because of the ubiquitous presence of anisotropic objects in living tissues, the transport of light in such systems has become a topic of interest and was investigated both theoretically [20,21] and experimentally in biological tissues [22,23]. The media investigated in those studies were solid, with no change in cell morphology and orientation. Given these recent advances, together with the size measurement capabilities demonstrated by these techniques [19], we endeavor to characterize as completely as possible several human red cell suspensions with "tuned" erythrocytes properties.

Using concentrated suspensions (40% in volume fraction) of red blood cells with manipulated properties, we show that techniques using incoherent light cannot only measure aggregate sizes, but also characterize simultaneously the average anisotropy of the medium. From a biological point of view, the measurements on red blood cell suspensions in physiological conditions presented here give quantitative information on their aggregability and deformability without dilution [24].

II. EXPERIMENTAL SETUP, METHODS, AND MATERIALS

A. Experimental setup

The rheo-optical experimental setup principles (Fig. 1) are described in details elsewhere [19,25]. It consists of a 1 mW laser diode (635 nm) with integrated optics which focus the laser at the sample surface (spot size 50 μm). The backscattered image (1 cm$\times$1 cm) is acquired through a CCD camera (Adimec: 12 bits, 1 Megapixels) and consists essentially of the incoherent part of the electromagnetic field. Indeed, the acquired images are much larger than both the laser beam size and the enhanced backscattering cone (a few mrad in our case). Also, speckles fluctuations contribute only to a few

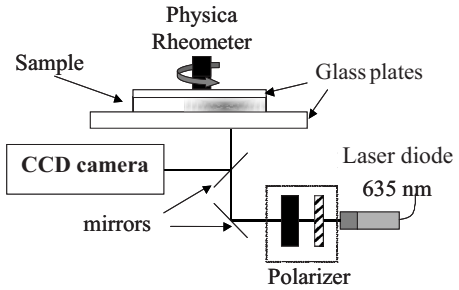

FIG. 1. Experimental setup. The incident light first enters a linear polarizer and then an electrically controlled liquid crystal retarder. The polarizer therefore generates, in particular, circular right and circular left polarizations.

*christophe.baravian@ensem.inpl-nancy.fr

percent of the intensity (for a detailed discussion, see [26]). In order to decrease speckles fluctuations, each image corresponds to the averaging of 10 images.

The shear is controlled by a rheometer (MCR 300 Physica, Anton Paar) in a specially designed parallel glass plate geometry (5 cm diameter and 3 mm gap). In the following, all experiments are performed under shear in a climatized room at 20 °C.

Finally, for image analysis purposes, we define the barycenter of the spatial intensity repartition as the coordinates origin.

B. Measurement of nonpolarized light transport

This work focuses on the transport of energy in an anisotropic medium, i.e., the transport of nonpolarized electromagnetic waves (EMW). To show that this is experimentally possible and is meaningful, a digression about Stokes formalism is necessary. In this formalism, an EMW is characterized by its Stokes vector $\mathbf{S}=(a,b,c,d)$ where a represents the energy of the EMW, the other parameters accounting for the different polarizations contributions. The Stokes vector of an EMW coming out of the medium is then simply: $S_j^o=\Sigma_{k=1}^4 M_{j,k}S_k^i$, where $\mathbf{S}^i$ and $\mathbf{S}^o$ are respectively the incoming and outgoing Stokes vector of the EMW. This relationship also defines the 4 by 4 Mueller matrix $\mathbf{M}_{j,k}$. In this representation, an incoming randomly polarized EMW (=unpolarized) is simply characterized by its energy (1, 0, 0, 0). Also, if no polarizer is put in front of the detector, as detectors only measure energy densities, it corresponds to multiplying the outgoing Stokes vector by (1, 0, 0, 0). Thus, by using an unpolarized incoming light and no polarizer in front of the detector, the $M_{11}=(1,0,0,0)\cdot\mathbf{M}\cdot(1,0,0,0)^T$ element of the Mueller matrix can be measured. Practically, it is very difficult to collimate unpolarized light as it usually originates from thermal sources with wide emission spectra. Fortunately, alternative ways of measuring M_{11} are feasible.

One consists in acquiring two images $I1$ and $I2$ with incoming Stokes vector of (1, 0, 0, 1) and $(1,0,0,-1)$, corresponding respectively to a circular left and circular right incident polarization, together with no polarizer in front of the camera. We have $I_1=(1,0,0,0)\cdot\mathbf{M}\cdot(1,0,0,1)^T=M_{1,1}+M_{1,4}$ and $I_2=(1,0,0,0)\cdot\mathbf{M}_{i,j}\cdot(1,0,0,-1)^T=M_{1,1}-M_{1,4}$. So $M_{1,1}=(I_1+I_2)/2$. In practice, the two incident polarizations are selected by a linear polarizer followed by an electrically controlled liquid crystal retarder (Meadowlark) calibrated using the methods described in [25] to generate circular polarizations $(1,0,0,\pm 1)$. The construction of an averaged nonpolarized image I (2×10 raw images) takes about 1 s.

C. Blood samples

The experiments were performed on prepared human blood samples close to physiological concentrations. About 100 mL of blood from a healthy donor was placed into ten 10 mL tubes and centrifuged three times, first at 3000 rpm for 10 min to remove the plasma, free hemoglobin and platelets. The erythrocytes were then suspended in a PBS buffer (Sigma). Two more centrifugation were performed at 2000 rpm for two minutes followed by a wash with PBS. The obtained suspension is nonaggregating and the final volume fraction in erythrocytes, determined from the hematocrite, is of $40\pm 1\%$.

TABLE I. Denomination and properties of the different blood samples.

Name	Aggregating	Hardened	Shape
D	No	No	Discoids
DA	Yes	No	Discoids
DH	No	Yes	Discoids
S	No	No	Spheroids
SH	No	Yes	Spheroids

Standard techniques were used to change the shape, the deformability and/or the aggregability of the erythrocytes suspensions. The PBS saline content allows to control the osmotic stress on the erythrocytes and thus the shape of the cells [27]. Adding glutaraldehyde at 0.05% to the suspension induces a hardening of the cells membrane, decreasing considerably their deformability [28]. Finally, dextran (3%) was added in one sample in order to simulate erythrocyte aggregation [29]. Thus five different samples types were produced as summarized in Table I.

III. UNPOLARIZED, INCOHERENT LIGHT TRANSPORT IN A SUSPENSION OF RANDOMLY ORIENTED DISKLIKE OBJECTS

A. Background

This section describes qualitatively the travel of a photon inside a random medium, and allows to define the numerous parameters necessary to describe this phenomenon.

When an incoherent photon packet enters a medium composed by a dispersion of microscopic objects, it first experiences an interaction with one of these objects. In this interaction, defined as a scattering event, the photon packet's energy is nonuniformly dispersed in space and may also be partially absorbed. This scattering event can be seen as a directional choice, made according to the scattering probability $P(\theta,\psi)$ [30], where θ is the angle between the incident and outgoing photon direction and ψ is the azimuthal angle.

1. Spherical scatterers

When the scatterers are spherical, this interaction is governed by two dimensionless parameters: The size parameter $x=2\pi RN_m/\lambda$ and the optical parameter $m=N_p/N_m$ where N_p is the particle refractive index. R is the volume average of the particles radii, λ the incident wavelength and N_m the surrounding medium refractive index. Also, for unpolarized photons, the probability function $P(\theta,\psi)$ does not depend on ψ, due to azimuthal symmetry. As the medium is composed of a collection of these objects, the photon packet, after a free flight on a characteristic distance $l_s=4/3\pi R^3/\phi C_{\mathrm{scat}}$, encounters another particle, is scattered (or absorbed) in a new direction and so on. The scattering length l_s depends on

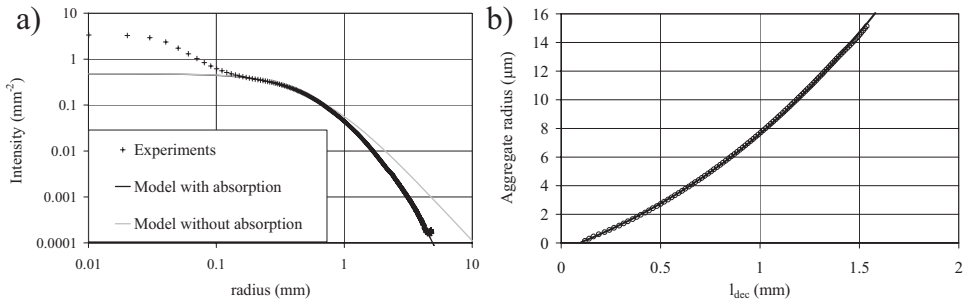

FIG. 2. (a) Radial distribution of the unpolarized incoherent backscattered intensity for sample D at rest. The continuous lines are fits of the absorbing and nonabsorbing models. (b) Evolution of the decorrelation length (mm) versus the scatterer radius (μm). Circles: Mie calculation for $m=1.045$ and $\phi=0.39$. Line: polynomial fit.

the particle volume fraction ϕ and on the scattering cross section $C_{\text{scat}}(x,m)$. Along this journey inside the medium, the photon progressively looses memory of where and how it entered the medium on a typical transport length l_{TR} defined as $1/l_{\text{TR}}=(1-g)/l_s+1/l_a$. g is the anisotropy factor and l_a the absorption length. Finally, some photons exit the medium in the backward direction and are detected by the camera.

2. Anisotropic scatterers

In the case of anisotropic particles however, the probability phase function $P(\theta,\psi)$ for a single scattering depends on ψ, even for unpolarized light. For instance, in the diffraction approximation, for directions parallel to a cylinder axis $P(\theta,0°)$ or perpendicular to this cylinder axis $P(\theta,90°)$, the ratio of the envelope $P(\theta,90°)/P(\theta,0°)=A^2$, where A is the ratio of the cylinder length to its diameter [30]. So, light is scattered more efficiently in a direction perpendicular to the cylinder axis. When anisotropic objects are globally oriented, the symmetry axis around the incident beam direction is lost. Thus an anisotropic light propagation is expected at large distances compared to the scattering length [20,21,23,31]. A corollary of this description is that randomly positioned and randomly oriented anisotropic objects should keep the polar symmetry of the macroscopic incoherent light transport. In other words the unpolarized incoherent light transport in such a nonoriented medium is equivalent to the transport in an effective medium composed of spherical objects.

B. ILT measurements: Volume average of erythrocyte size

A sample composed of nonaggregating erythrocytes with their normal disklike shape ("D" sample in Table I) is studied here. Incoherent light transport measurements were made at rest (zero shear rate) using a container of radius 2 cm and height 10 mm to ensure that the semi-infinite medium approximation is valid for incoherent light transport [26]. The image obtained from the camera was axisymmetric, confirming the qualitative description presented above. After angular integration, the intensity curve shown in Fig. 2(a) was obtained.

1. Absorption

The radial intensity distributions [Fig. 2(a)] were fitted using the following semi-infinite diffusion model including absorption [5,32]:

$$I(r)=\frac{1}{l_{\text{TR}}^2}\left\{e^{-\mu l_{\text{TR}} r_1}\left[\frac{a}{r_1^2}\left(\frac{1}{r_1}+\mu\right)+\frac{b}{r_1}\right]+e^{-\mu l_{\text{TR}} r_2}\left[\frac{d}{r_2^2}\left(\frac{1}{r_2}+\mu\right)-\frac{b}{r_2}\right]\right\}, \quad (1)$$

with $r_1=\sqrt{1+(r/l_{\text{TR}})^2}$, $r_2=\sqrt{c+(r/l_{\text{TR}})^2}$, and $\mu=\sqrt{3/l_a l_{\text{TR}}}$. Since the glass plates are treated to avoid reflection, we have the following parameter values: $a=0.0398$, $b=0.0597$, $c=5.4444$, and $d=0.09284$. The gray curve in Fig. 2(a) corresponds to the fit when forcing the absorption coefficient to zero and the other one with the absorption as a free parameter. The latter fits the data very well as shown in Fig. 2(a) which means that, unsurprisingly, the blood sample absorbs light significantly at 635 nm. A transport length of $l_{\text{TR}}=0.41$ mm and an absorption length of $l_a=14$ mm are obtained, consistently with values obtained by Ishimaru [7]. Measurements of this absorption length can be related to the oxygen saturation of the hemoglobin present in the cells as shown in [7,33].

2. Size inversion

As the optical index ratio and the measured volume fraction of the cells are known, it is possible with some caution to use the above lengths and Mie theory to deduce a volume average size for the suspended objects [18,19,34]. In those studies, the materials were nonabsorbing ($l_a=\infty$), so that the size determination was performed directly on the transport length. For absorbing samples, since $1/l_{\text{TR}}=(1-g)/l_s+1/l_a$, the inversion must be performed on the decorrelation length defined as $l_{\text{dec}}=l_s/(1-g)$. Since the considered size range (above 1 μm) is larger than the wavelength ($x>1$), the theoretical evolution of this decorrelation length with the object size is biunivocal [see Fig. 2(b)]. This evolution is calculated using Mie theory applied to spheres with the appropriate optical index ($m=1.045$) and volume fraction ($\phi=0.39$). It is fitted using a simple polynomial giving the following relationship between the decorrelation length and the average spherical equivalent size of the objects: $R_{\text{eq}}=3.77l_{\text{dec}}^2+4.26l_{\text{dec}}-0.35$ with R in μm and l_{dec} in mm.

As $l_{\text{dec}}=0.422$ mm, a value of $R_{\text{eq}}=2.1$ μm is found for the equivalent spherical radius of an erythrocyte, in correct agreement with standard estimates. Indeed, the average volume of an erythrocyte is about 60 μm^3 which gives an equivalent spherical radius of 2.4 μm. The difference may be due to inaccuracies in the determination of the refractive in-

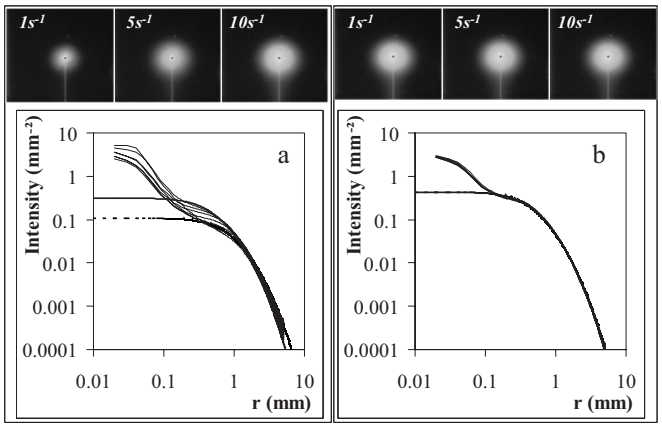

FIG. 3. Radial intensity decrease from the image barycenter at shear rates of 2, 5, 10, 20, 50, 100, and 200 s^{-1}. ϕ=0.39. (a) Aggregating sample (DA) and (b) nonaggregating sample (D). Thick lines correspond to fit of Eq. (1) on the data obtained at 5 s^{-1} (dashed) and 200 s^{-1} (continuous).

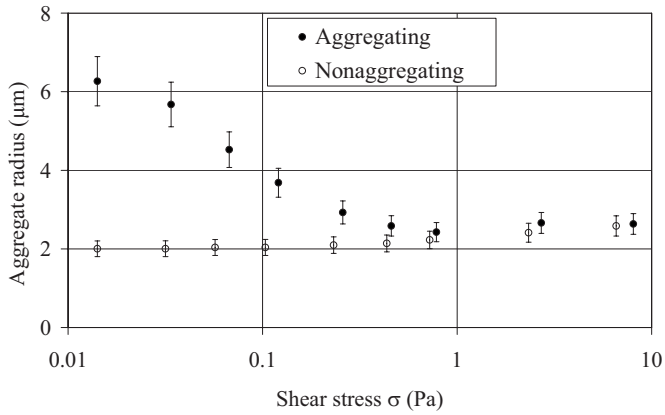

FIG. 4. Aggregate radius versus shear for aggregating (closed symbols) and nonaggregating (open symbols) blood suspensions. ϕ=0.39.

dex or (and) to the fact that an erythrocyte is not a homogeneous object.

IV. AGGREGATE SIZE MEASUREMENTS IN SIMULATED AGGREGATING BLOOD

One of the main properties of red blood cells is their aggregability. Incoherent light transport measurements were performed under varying shear for two discoids samples, the aggregating (DA) and the nonaggregating one (D).

The images at the top of Fig. 3 correspond to nonpolarized $[I=(I_1+I_2)/2]$ intensity images at three different shear rates for the aggregating sample (left) and the nonaggregating sample (right), showing a clear difference in the light transport evolution for the two samples. Figure 3 shows the angularly averaged radial intensity distributions, for all seven shear rates applied to (a) the aggregating sample and (b) the nonaggregating sample. The first obvious observation is that all curves for the nonaggregating sample are almost identical, whereas there is a clear difference for the aggregating one.

The data are fitted with the same semi-infinite depth model including absorption as previously [Eq. (1)]. Indeed, the depth of the sample in those experiments is of 3 mm, still much larger than the measured decorrelation lengths. To verify this, the much more elaborate finite depth model developed in [26] was also used to fit these data (not shown), with no significant differences in the obtained absorption and decorrelation lengths. The absorption length is still of 14 mm and, as expected, is independent of aggregation.

If we suppose that the aggregates are very compact, then the volume fraction of objects remains constant, allowing to calculate an equivalent object size from the decorrelation length, as shown above. In Fig. 4 the equivalent average object size is plotted against the shear stress for both the aggregating (closed symbols) and the nonaggregating samples (open symbols). There is an obvious difference in average scatterers size between the two samples, the size of the objects in the nonaggregating sample staying almost constant, close to an individual cell size. In the aggregating sample, the size of the scattering objects in the suspension decreases while increasing the shear stress, showing the well known shear-induced desaggregation. At vanishing shear stresses, the aggregates have an equivalent spherical radius of about 6 μm, corresponding to aggregates of approximately 30 cells in average (Fig. 4). When increasing the shear stresses, the aggregates size decreases progressively down to individual cells with an equivalent volume radius of 2.2 μm, joining the nonaggregating sample at high shear stresses. Upon close inspection, a slight (20%) increase of the average size of the nonaggregating sample is observed above shear stresses of 1 Pa, increase which actually occurs simultaneously to a deformation of the images. This phenomenon will be discussed in the final section of this paper.

In conclusion of this part, the analysis of the spatial repartition of incoherent nonpolarized photons backscattered from a red blood cell suspension gives quantitative informations about the size and absorbance of the scatterers met by the photons. In the experiments presented here, the scatterer's size evolution with shear describes the decrease of aggregates sizes with increasing shear from which an aggregation constant could be deduced. Also, as we measure independently the absorption length in the suspension, the oxygen saturation of the hemoglobin in the red cells could be deduced [7].

V. LIGHT TRANSPORT IN ANISOTROPIC TURBID MEDIA

A. Qualitative evidence of anisotropic long range effects

To show qualitatively the effect of shear, raw images $I=(I_1+I_2)/2$ of the unpolarized backscattered intensity obtained at different shear rates is shown in Fig. 5(a), for the discoid nonaggregating suspension ("D" sample). The image slightly deforms with increasing shear. To show the effect more clearly, the difference between the image at a given shear rate minus the one at 10 s^{-1} is presented in Fig. 5(b). We observe the appearance of a "butterfly" pattern which

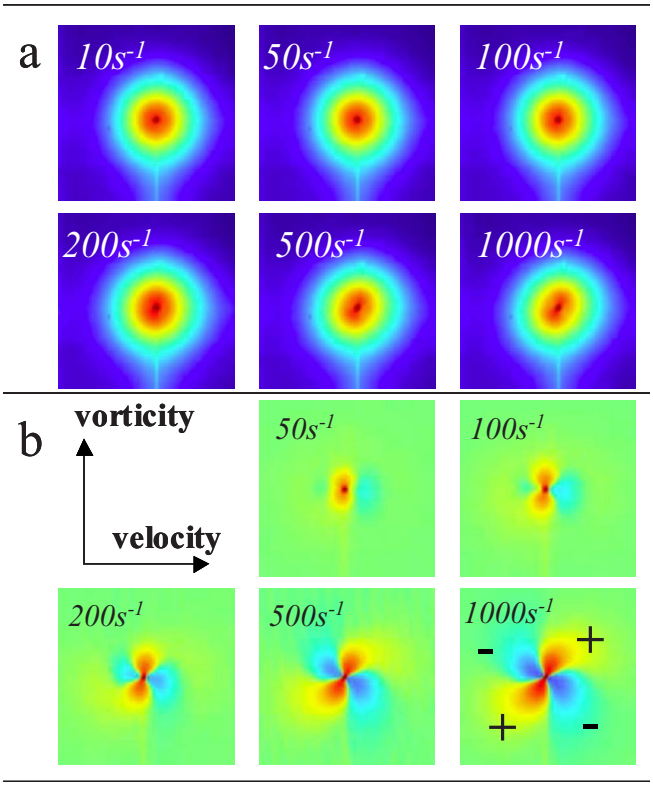

FIG. 5. (Color online) Anisotropy of backscattered light for spherical blood cells. (a) Logarithmic representation of images for different shear rates. (b) Differences between images at different shear rates and the image at 10 s^{-1}. Intensity amplitude is in arbitrary units. The negative lobes define the deformation axis. $\phi = 0.39$.

should *not* be mistaken with those observed in polarized light transport situations. As explained in the experimental setup description, the M_{11} element of the Mueller matrix is measured which corresponds strictly to the energy transport.

As shown both experimentally [23] and theoretically [20], the origin of this anisotropy of the incoherent light transport is the consequence of the collective orientation of anisotropic objects. In our case, the anisotropy of incoherent light transport is produced by the deformation and global orientation of red cells, averaged both in time (over 1 s) and in space (over a volume sample of a few mm^3). This observation of anisotropic incoherent light transport in an oriented media is similar to the one of Kienle *et al.* [23], and to the anisotropy observed in strongly scattering media using coherent light [35,36], or to the order parameter determined from x-ray [37] or neutron experiments. Interestingly, all the experimental and theoretical studies cited above investigated cylinderlike structures. We observe the anisotropy of incoherent light transport induced by oriented disklike objects which may have behaved differently because of the symmetry differences.

B. Determination of the deformation and orientation of modified blood cells under shear

In the following experiments, four nonaggregating blood samples are used, one with normal deformable discoid cells

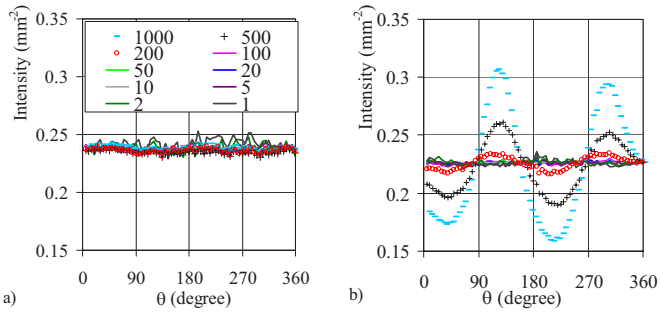

FIG. 6. (Color online) Evolution of the intensity amplitude measured at l_{TR} for varying shear rates (in s^{-1}). (a) Hardened discoid cells (DH). (b) Normal discoid cells (D).

("D"), one with deformable spherical cells ("S"), the last two with nondeformable discoid ("DH") and spherical cells ("SH").

1. Determination of the anisotropy index of the erythrocytes suspensions

From the diffusion theory of Heino *et al.* [20] concerning unpolarized radiative transfer in anisotropic media, it appears that such a medium may be characterized by the ratio between two transport lengths. Thus we simply determine the intensity oscillation amplitude at a radius equal to the transport length (l_{TR}) from the barycenter of the image. Such oscillations in light intensity measured at a radius l_{TR} are shown in Fig. 6 for both the hardened [Fig. 6(a)] and the nonhardened samples [Fig. 6(b)] clearly showing a quantifiable difference. The amplitude of the oscillation divided by the average value is measured by fitting a sine function. It is called the "anisotropy index." Several other methods were tried and always gave measurements proportional to the one we chose.

This measurement method is applied to the images obtained for various shear applied to the different nonaggregating samples. The resulting anisotropy indexes are plotted against applied shear stress in Fig. 7. The measured index is almost zero for hardened cells, whatever their geometry,

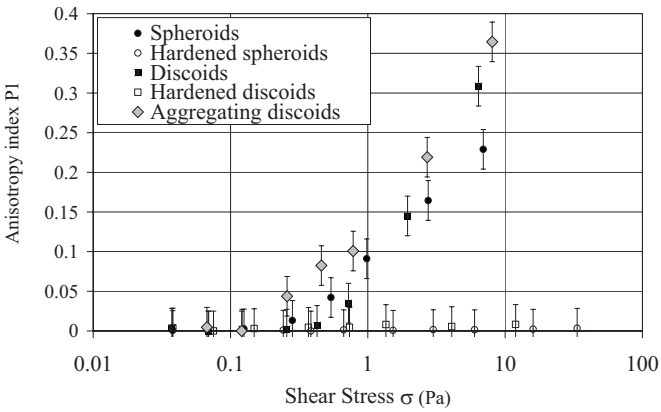

FIG. 7. Index of anisotropy measured for the different samples at various shear stresses. Closed symbols correspond to normal cells, while open symbols correspond to hardened cells. Diamonds correspond to the aggregating deformable discoids ("DA sample").

while it strongly increases for standard deformable cells. The first conclusion of these measurements is that, in the suspension under consideration and in the actual experimental geometry, the development of an optical anisotropy is a consequence of the deformability of the cells.

However, the hardened discoid cells do not seem to orient under flow as they should at such high concentrations. The interpretation of this *a priori* surprising result asks for a careful assessment of the flow and optical geometries.

2. Deformation and orientation of erythrocytes under shear

From elementary geometrical consideration, it is clear that the unpolarized incoherent light transport setup used here is only sensitive to orientations and deformations with their main anisotropy axis *in* the observation plane. In consequence, since normal erythrocytes in suspensions are known to orient in the plane of shear [38,39] (i.e., with their main anisotropy axis *perpendicular* to the observation plane), it is likely that the deformation observed in Fig. 5 corresponds to the threadlike deformation where the discoids elongate with their surface facing the shear plane and their main elongation axis in the flow direction [40]. The curve displaying the index of deformation of spheroids (Fig. 7) shows that they also undergo a deformation and an orientation in the plane of shear, in agreement with existing work (see, e.g. [41]). Concerning hardened erythrocytes, because of the geometrical constraints of our setup, it is quite normal that no orientation is observed, as they may either tumble [42] or simply orientate in the plane of shear, the difference being impervious to our measurement method.

The anisotropy induced patterns shown in Fig. 5 also give quantitative informations on how the cells deform and orient under shear. First, the negative lobes gives the main alignment axis [Fig. 5(b)], showing that the deformation axis of the cells is almost aligned with the velocity direction at all shear rates. Further, as shear increases, the anisotropy index also increases, in good agreement with measurements performed using diffraction methods in dilute conditions [24], and with very similar accuracies. Finally, it appears that the cells start to deform for shear stresses between 0.1 and 1 Pa, again in good agreement with existing measurements [24].

C. Simultaneous disaggregation and deformation of erythrocytes

It was observed in Sec. IV that the aggregating deformable samples ("DA" sample) did not only disaggregate under shear but also developed an anisotropy together with an apparent size increase for shear stresses larger than 1 Pa. In Fig. 7, the anisotropy index for this sample is also plotted, showing that the anisotropy of the aggregating cells is similar to that of the nonaggregating cells. Comparing graphs 4 and 7 shows that the deformation starts at shear stresses where the aggregates have been destroyed since their size is close to that of a single cell.

Concerning the increase of apparent size of the cells, this could be the consequence of either a true increase in the volume of the sheared erythrocytes or to an effect of erythrocytes orientation in the plane of observation, slightly modifying the light transport. Even if erythrocytes deformation is usually modeled using volume conserving models (e.g., [40]) some measurements have shown that the surface and the volume of the erythrocytes increase at high shear rates [43,44]. It then looks more likely that the observed equivalent size increase is the consequence of the increased volume size of the cells due to their deformation.

VI. CONCLUSION

In conclusion, the careful analysis of steady incoherent unpolarized light transport in sheared blood samples allowed the quantification of most properties of the suspended cells, for conditions close to standard whole blood physiological conditions. Indeed, both the typical cells and aggregates size evolution versus shear stress were obtained and, simultaneously, the orientation and deformation of those cells. As such, the method presented here may prove a very powerful tool to discriminate between normal or diseased blood as anormal values of these properties can be linked to severe illnesses.

More generally, the modified blood samples studied in this work can also be seen as model suspensions of anisotropic objects since the properties of the suspended erythrocytes are well controlled. The optical technique used in this article could then be used to investigate the properties of concentrated colloidal suspensions, in particular those made of anisotropic objects that may orient under the action of an external field such as gravity, electromagnetic fields or shear. However, some more theoretical work is needed to relate quantitatively the measured anisotropies to the objects shape and their orientation.

ACKNOWLEDGMENT

We thank Anton Paar for lending the rheometer used in this study.

[1] L. Reynolds, C. C. Johnson, and A. Ishimaru, Appl. Opt. **15**, 2059 (1976).
[2] R. Aronson, J. Opt. Soc. Am. A **12**, 2532 (1995).
[3] M. Dogariu and T. Asakura, Waves Random Media **4**, 429 (1994).
[4] D. Durian and J. Rudnick, J. Opt. Soc. Am. A **16**, 837 (1999).
[5] R. Haskell, L. Svaasand, T. TSay, T. Feng, and S. McAdams, J. Opt. Soc. Am. A **11**, 2727 (1994).
[6] J. R. Mourant, J. Freyer, A. Hielscher, A. Eick, D. Shen, and T. Johnson, Appl. Opt. **37**, 3586 (1998).
[7] A. Ishimaru, *Wave Propagation and Scattering in Random Media* (IEEE Press, Piscataway, New Jersey and Oxford

University Press, New York, 1997).
[8] S. Bartel and A. H. Hielscher, Appl. Opt. **39**, 1580 (2005).
[9] P. E. Wolf and G. Maret, Phys. Rev. Lett. **55**, 2696 (1985).
[10] D. J. Pine, D. A. Weitz, P. M. Chaikin, and E. Herbolzheimer, Phys. Rev. Lett. **60**, 1134 (1988).
[11] J. Z. Xue, D. J. Pine, S. T. Milner, X.-l. Wu, and P. M. Chaikin, Phys. Rev. A **46**, 6550 (1992).
[12] A. Polishchuk, T. Dolne, F. Liu, and R. Alfana, J. Opt. Soc. Am. A **22**, 430 (1997).
[13] S. Arridge, Inverse Probl. **15**, R41 (1999).
[14] J. Paasschens, Ph.D. thesis, Leiden University, Netherlands, 1997.
[15] S. Prahl, Ph.D. thesis, University of Texas, USA, http://www.bme.ogi.edu/prahl/pubs/abs/prahl88.html (1988).
[16] X. Wang, L. Wang, C.-W. Sun, and C.-C. Yang, J. Biomed. Opt. **8**, 608 (2003).
[17] F. Morin, R. Borrega, M. Cloitre, and D. Durian, Appl. Opt. **41**, 6294 (1999).
[18] J. Mougel, O. Alvarez, C. Baravian, F. Caton, P. Marchal, M.-J. Stebe, and L. Choplin, Rheol. Acta **45**, 555 (2006).
[19] C. Baravian, F. Caton, J. Dillet, and J. Mougel, Phys. Rev. E **71**, 066603 (2005).
[20] J. Heino, S. Arridge, J. Sikora, and E. Sommersalo, Phys. Rev. E **68**, 031908 (2003).
[21] J. Heiskala, T. Neuvonen, P. E. Grant, and I. Nissilä, Appl. Opt. **46**, 1633 (2007).
[22] G. Marquez, G. Maret, L. V. Wang, S.-P. Lin, J. A. Schwartz, and S. L. Thomsen, Appl. Opt. **37**, 798 (1998).
[23] A. Kienle, F. K. Forster, and R. Hibst, Opt. Lett. **29**, 2617 (2004).
[24] X. Wang, H. Zhao, F. Y. Zuang, and J. F. Stolz, Clin. Hemorheol Microcirc **21**, 291 (1999).
[25] J. Dillet, C. Baravian, and F. Caton., Appl. Opt. **45**, 4669 (2006).
[26] F. Caton, C. Baravian, and J. Mougel, Opt. Express **15**, 2847 (2007).
[27] P. Canham and D. R. Parkinson, Can. J. Physiol. Pharmacol. **48**, 369 (1970).
[28] R. Carr and G. R. Cokelet, J. Rheol. **25**, 67 (1981).
[29] J. Hardwicke, C. R. Ricketts, and J. R. Squire, Nature (London) **166**, 988 (1950).
[30] C. Bohren and D. Huffman, *Absorption and Scattering of Light by Small Particles* (Wiley and Sons, New York, 1983).
[31] O. K. Dudko and G. H. Weiss, Biophys. J. **88**, 32053211 (2005).
[32] A. Kienle and M. Patterson, J. Opt. Soc. Am. A **14**, 246 (1997).
[33] R. J. Hunter, M. S. Patterson, T. J. Farrell, and J. E. Hayward, Phys. Med. Biol. **47**, 193 (2002).
[34] C. Baravian, J. Mougel, A. Durand, and F. Caton, AIChE J. **53**, 1994 (2007).
[35] P. M. Johnson, B. P. J. Bret, J. Gomez Rivas, J. J. Kelly, and A. Lagendijk, Phys. Rev. Lett. **89**, 243901 (2002).
[36] R. Sapienza, S. Mujumdar, C. Cheung, A. G. Yodh, and D. Wiersma, Phys. Rev. Lett. **92**, 033903 (2004).
[37] M. Deutsch, Phys. Rev. A **44**, 8264 (1991).
[38] D. E. McMillan, N. G. Utterback, and M. Lee, Biorheology **25**, 675 (1988).
[39] M. Fujii, K. Nakajima, K. Sakamoto, and H. Kanai, Ann. N.Y. Acad. Sci. **873**, 245 (1999).
[40] S. Noji, H. Kon, and S. Taniguchi, Appl. Opt. **46**, 349355 (1984).
[41] S. Ramanujan and C. Pozrikidis, J. Fluid Mech. **361**, 117 (1998).
[42] M. Bitbol, Biophys. J. **49**, 1055 (1986).
[43] A. W. Jay and P. B. Canham, Biophys. J. **17**, 169178 (1977).
[44] G. Lenormand, S. Hénon, A. Richert, J. Siméon, and F. Gallet, Biophys. J. **81**, 4356 (2001).